RAL-TR-1998-059

THE OPERATION OF VACUUM PHOTOTRIODES IN AN AXIAL MAGNETIC FIELD - A MONTE-CARLO STUDY

J.E.Bateman

Rutherford Appleton Laboratory, Chilton, Didcot, OX11 0QX

11 August 1998

ABSTRACT

The predictions of a simple monte-carlo model of the operation of vacuum photo-triodes in an axial magnetic field are presented and compared to some available experimental measurements.

1. INTRODUCTION

In the course of early testing procedures on some of the vacuum phototriodes (VPT) proposed for application in the ECAL Endcap it appeared that while superficially simple in construction it was not obvious what parameters controlled the essential property of interest for this application - namely the magnetic hardness of the gain. The inherent simplicity (and calculability) of the motion in combined electric and magnetic fields provoked the thought that a simple monte-carlo model may be able to elucidate the basic operating mode of the device and help with a rational design specification. The results presented below will, one hopes, contribute to the understanding and the design efforts, though as will appear, the effort to deliver a reasonably realistic model of the amplification process is quite substantial and not the simple exercise which it first appeared.

There are several parameters crucial to VPT operation (e.g. the secondary emission coefficient) which are dependent on processing (and) or commercially sensitive so comparison with experimental results is essential for calibration. The experimental data used comes from Hamamatsu data sheets, various presentations of results of the RIE devices and (most usefully) the measurements done by Derek Imrie and Peter Hobson at Brunel University.

The monte-carlo model is not presented as a perfected work of art, rather as an ongoing development (modelling the case of an angled B-field is still to be undertaken); but it is hoped that the results to date provide some insights into the operation of VPTs in an axial magnetic field. The geometry of the model is strictly planar with E and B fields only in the axial direction. Thus it cannot take account of edge effects due to non-axial components of either field and so, **in comparisons with experimental data its relevance is restricted to "centre field" data.**

2. THE BASIC MODEL

Figure 1 shows the basic structure of a VPT. Photoelectrons liberated from a semi-transparent cathode are accelerated by the potential difference V_c across the gap D_{ac} (usually about 3-4mm) to a mesh anode (set at earth potential) which has a geometric transparency (T_r) of the order of 50%. Those that penetrate the anode traverse the gap D_{ad} (1-3mm) through a decelerating potential drop V_d (about 200V) and generate secondary electrons in a high-gain dynode. These spray out towards the anode to which they are accelerated by V_d and a fraction are captured so generating the output signal in the anode circuit. Those secondaries penetrating the anode are de-accelerated in the anode-cathode gap and return to the anode where a fraction again adds to the output signal while the remainder return to the dynode and generate a further (decreasing) contribution of tertiary electrons which repeat the process. At each stage the energy spectrum of the returning electrons is degraded so that eventually the cascade stops.

In the case of low transparency anode meshes (35%) the cascade dies out very rapidly and tertiary electrons contribute only about 1% to the signal; but in the case of high transparency (70%) there can be nearly 10% in the tertiary electrons and a finite

quaternary signal. Flight times are typically of the order of 0.2 - 0.5ns in a gap so that the signal spread in the whole process is little more than 1ns.

The basic problem of the VPT is that the photo-electrons are required to pass through the anode mesh on the way to the dynode but the secondaries are required to hit it in order to generate an output signal. Since the motion of the electrons in the electric field is entirely conservative it is possible for an electron to oscillate through the anode mesh until it has spent all its initial energy in the dynode without ever generating an output signal. The electron kinematics are disrupted by the polar spread of the secondaries which (with typical bias conditions) spreads the secondaries from one primary over a circle of a few hundred microns on arrival at the anode plane. This enables an adequately fine mesh to sample the distribution and capture the expected fraction. The intuitive response to this mechanism is to suggest that a mesh transparency of 50% should be optimum; and this turns out to be true to first order.

If the anode mesh is sufficiently fine the electric field structure can be well approximated by V/D in each gap. Calculations for a similar field structure in wire counters [1] shows that in a typical VPT the field has this value (to a few %) over all of the gap more than a mesh pitch from the anode. Since mesh pitches are typically 0.05mm or less and the gaps ≥2mm the constant field approximation is good for >97% of the gaps. A further consideration in favour of the approximation is the fact that the electrons are moving fast at each approach to the anode and respond weakly to the attractive field around each mesh wire. Thus as a first approximation the constant field assumption is valid. However, as will be discussed below the attractive electrostatic forces around the wires do become important at high magnetic field values when only photoelectrons passing within a (mean) secondary cyclotron radius (a few microns above B=1T) of a mesh wire can generate secondaries which have a chance of impacting a mesh wire and generating an output signal.

2.1 Electron motion in an axial magnetic field

When an axial magnetic field is applied (i.e. parallel to the electric fields) the motion remains relatively simple. The motion along the x-axis (E-field direction) is unaffected by the B-field and is calculated using the simple kinetics for motion in constant acceleration (deceleration). In the transverse plane, any tranverse velocity component (v_T) gives rise to a cyclotron motion in a circle of radius ρ ($=mv_T/Be$) with an invariant period τ ($= 2\pi m/Be$).

With an electron energy of 5eV, $\rho=7.5\text{x}10^{-6}\sin\alpha/B$ meters where α is the angle the initial electron velocity vector makes with the x-axis. Thus in the earth's magnetic field ρ is centimeters and does not affect the motion much. At a magnetic field of 1T however, ρ is of the order of microns and dominates the motion. The cyclotron period τ is 0.0357/B ns. At values of B approaching 0.1T, τ becomes comparable with the flight time of electrons in the anode-dynode gap and resonance effects become evident. The motion of any electron in the y-z plane is thus simply a circle described with uniform angular velocity $2\pi/\tau$. The initial coordinates and velocity components specify the point on the circle and the position of the centre of rotation.

The motion of an electron is calculated in each free-flight transit by solving the quadratic equation for the time of flight (under constant acceleration) along the x-axis (T_f) and calculating the phase advance of the circular motion ($2\pi T_f/\tau$) to get the y and z coordinates at the end of the transit. When an electron passes through the anode mesh into a reversed E-field the transverse motion is unaffected (neglecting local mesh E-fields as described above) and the calculation is as before. The main problem in keeping track of the electron cascade is in preserving good housekeeping for the initial conditions of each section of motion.

The motion falls into three distinct mathematical cases: uniformly accelerated motion in region 1 of figure 1 (photoelectrons on first transit), uniformly retarded motion in region 2 (photo- or secondary electrons heading for the dynode) and ballistic reflection in region 1 (secondaries which escaped capture on the anode and are returned to the anode by the reverse field).

At the photocathode, and on the impact of an electron with the dynode fresh populations of electrons are created with new, randomised velocity vectors and each one must be tracked through the tube until it impacts on the anode mesh or fails to produce a secondary as it buries itself finally in the dynode.

These calculations are simple so permitting the tracking of several generations of electrons without incurring unacceptable processing requirements. The calculation of one gain point for 1000 photoelectrons takes typically 20 seconds using a Pentium Pro 200.

3. ELECTRON-SURFACE INTERACTIONS

Electron-surface interactions are vital to the operation of the VPT. They are not so simple to deal with as the electron motion problem, reflecting as they do complex solid-state interactions. Fortunately the stochastic nature of the electron solid interactions permit the use of simple statistical models (based firmly on experimental data).

3.1 The photoelectron spectrum

The spectral maximum of the light emission from lead tungstate corresponds to a photon energy of about 2.6eV. The photoelectron spectrum from the CsSb cathode was approximated by an exponential distribution with a mean energy of 0.75eV and a $\cos\theta$ spatial distribution in polar angle. In view of the typical values used for V_c (800-1000V) and the consequently negligible effect of any tranverse energy no attempt was made to make the photo-electric spectrum more realistic.

3.2 The secondary electron spectrum

On impact on the dynode a primary electron has an energy of V_c-V_d which (in the operating region) will amount to some 600-800eV. This energy produces a secondary spectrum which, while peaking at a few eV, stretches all the way up to the full energy where we see elastically scattered primaries. In the mid energy range (around 500eV)

we see inelastically scattered primaries which can be a large fraction of the primaries and which we must find a practical means to model in addition to the "genuine" secondaries at the low end.

Studying the results of Dressler [2] on beta backscattering shows that at the energies of concern to us (below 1000eV) and in the range of target atomic numbers relevant to us (Ni up to Ta) approximately 30% of incident electrons are backscattered with a mean energy of about 70% of the incident energy with an approximately gaussian distribution of width ≈0.3 of the incident energy and spatially distributed in a cosθ distribution relative to the reciprocal of the incident direction. Thus the model for the secondary emission process was divided into two stages: first the incident electron is allotted by a random weighting to either the backscattered (BS) or non-backscattered (NBS) category. In the latter case all the energy is used in the low energy secondary model (see below) while in the former the energy of the backscattered electron is calculated and that electron tracked back through the VPT while the residual energy is used to generate the low-energy spectrum appropriate to this energy. When the energy assigned to the backscatter exceeds the incident energy it is assigned to that energy. This yields a plausible elastic scatter peak.

In order to model the low energy secondary electron (SE) spectrum one turns to the extensive literature of which the data of Kollath [3] is typical. This reference gives SE spectra for Mo (Z=42) and Ta (Z=73) straddling our Z region of interest for CsSb (51-55). The distributions both peak at 2eV and only the high energy tails differ slightly. Experimentation shows that the distributions can be reasonably well modelled with either a log-normal distribution or a difference of exponentials, either of which can be modelled statistically with ease. The latter function was chosen with values of 1eV and 5eV for the exponential scale constants (figure 3) i.e.

$$\frac{dN}{dE_s} = \text{const}\left(e^{-Es/5} - e^{-Es/1} \right)$$

where E_s is the SE energy in eV.

The final problem is to evaluate how many secondaries samples should be generated for any given energy deposit in the dynode. The simple model of secondary emission based on an exponential escape depth for the SE s works well when compared with experiment. The number of electrons emitted for an incident energy E_p is [4]:

$$n(E_p) = 1/w \int_0^{R_p(E_p)} dE/dx \; e^{-x/\lambda} \; dx$$

where w is the energy required to ionise one electron, dE/dx is the energy loss per unit length in the material, R(E) is the range energy relationship of the primary electrons in the material and λ is the escape depth of the secondary electrons. Below E_p=1keV dE/dx is approximately constant and R≈kE. Hence:

$$n(E_p) \approx \lambda/kw\{1 - e^{-kE_p/\lambda}\}$$

i.e. we require two constants (to be obtained by fitting experimental data), ε_{max} (=λ/kw) the maximum number of secondaries obtainable (known as the secondary emission coefficient) and ε_{scale} (=λ/k) a characteristic energy of the surface.

Figure 2 shows a comparison of the gain calculated by the model (B=0) as a function of the incident electron energy on the dynode with the measured gain of one of the prototype tubes. Good agreement is achieved with ε_{max}=35.9 and ε_{scale}=304eV. These values hold good (within 10%) for all the tubes modelled which confirms the assumption that they all use CsSb dynodes.

A running total of the energy contained in all the secondaries generated by one primary is maintained to ensure that the non-physical situation of this exceeding the incident energy cannot arise.

The secondary electron spectrum generated by this algorithm is illustrated in figure 3 for an incident energy of 600eV.

3.3 Backscattering on the anode mesh.

In the model the "capture" of an electron by the anode is represented by the y,z coordinates of the particle orbit at x=0 (the anode mesh) occurring in the space occupied by metal in a model of the mesh structure. As noted with the interaction of an electron with the dynode the interaction with the anode is not so simple. The typical anode mesh materials (Ni and Cu) and their coatings (Sb and Cs) are capable of generating back scattering at the level of >20% . Since this contributes a randomizing factor to the electron paths it was thought important to incorporate this effect in the model.

The same model as applied to the dynode is applied to each interaction with the anode. The backscattered electron is then tracked through the VPT until finally absorbed in the anode or the dynode. The backscattered fractions can be adjusted independently to account for differences in the dynode and anode materials (though the Dressler results indicate that there is little significant difference over the range of Z involved).

4. MAGNETIC MATERIALS

Many materials used structurally in phototubes are ferromagnetic in some degree. For example Ni will saturate with a polarisation field of 0.55T at a driving field of 5000A/m (30mT in air). A Ni anode mesh will thus "attract" field lines and thus electrons until the material is saturated around B=0.5T. Similarly magnetic materials used for the mesh support rings and legs will distort the B-field near the edges of the active area and (generally) cause a loss of signal. The model cannot take account of such effects.

5. EXPERIMENTAL AND MANUFACTURING TOLERANCES

The mathematical calculations of the model are extremely precise on the scale of the practical VPT and the experimental set-up. This can lead to effects which may not be observed in practice. In order to explore these effects provision has been made in the model to (i) modulate the anode mesh position with a gaussian error which can be set to any hypothesised tolerance (ii) modulate the B-field in a similar manner to take account of field non-uniformity in the experimental set-up. At present only changes in magnitude are imposed, not changes in orientation.

6. RESULTS

The model can be used to explore the complete range of properties of a model VPT - gain, excess noise factor and timing. When confidence in the model is established the controllable manufacturing parameters can be varied to seek for the optimal solution to the magnetic hardness problem. In this report the main aim is to compare the model responses with the experimental measurements currently available in order to establish this confidence. Two parameters are presented - the multiplication gain (M) and the excess noise factor (F) as a function of the axial magnetic field.

While the cathode and dynode gaps vary within a range of ±1mm for the various tubes the important parameters are the frequency of the mesh pattern (L) in lines/mm and the geometric transparency of the mesh (T_r).

GAIN MEASUREMENTS

6.1 Electron Tubes VPT No.100001 (L=15.7 lpmm, T_r=0.6)

Figure 4a shows some gain curves measured at Brunel University for this tube (up to B=0.4T) with the output from the model superimposed. The general trend of agreement is good but the resonant behaviour of the model is more extreme than that of the experimental data. Figure 4b shows the model rerun with gaussian errors of 5% imposed on the B-field and 0.05mm on the anode position.

6.2 RIE VPT No. FEU-189-137 (L=30 lpmm, T_r=0.7)

Figure 5 shows the model compared with the curve presented for an RIE tube at the last CMS meeting. This is a relative gain plot: the model gain at B=0 is 14.3. The agreement is good in the general trend but, as in the previous case, shows more oscillations. The model results are extended from B=1.3T to B=4T.

6.3 Hamamatsu R2148 Variants

Figure 6a shows the relative gain versus B-field for the basic R2148 up to 1T (L=30 lpmm, T_r=0.7) as specified in the Hamamatsu data sheet. The mesh and spacing parameters are assumed to be the same as those measured at Brunel University. The

actual gain at B=0 calculated by the model is 12.1 in good agreement with the data sheet.

A fine-mesh variant of the R2148 was measured at Brunel - MODXA0568 (L=78.7 lines/mm, T_r=0.35) up to B=0.4T. Figure 6b shows the comparison with the model. The model gain at B=0 is 11.3.

7. EXCESS NOISE MEASUREMENTS

The excess noise factor may be evaluated in various ways. In terms of the single electron response function (SERF) (the distribution of electrons (i.e. gains) produced by a single photoelectron) it is defined as follows:

$$F = 1 + \sigma_{rel}^2$$

where σ_{rel} is the standard deviation of the SERF expressed as a fraction of the mean. The model is arranged to calculate the gain of single PE events 2000 times, histogram the results and calculate F as above.

Figures 7a and 7b show the model results of F as a function of B plotted against the values measured at Brunel for the Electron Tubes #10001 in two different bias configurations.

The SERFs give an explicit picture of the signal dispersion which produces the large F values. Figure 8a shows the SERF recorded for this VPT at B=0 and figure 8b that for the Hamamatsu R2148MODXA0568.

8. USING THE MODEL TO COMPARE TWO VPT DESIGNS

With some confidence that the model is capable of reproducing the behaviour of a VPT the model can be used to calculate the behaviour in regions of B-field outside the experimental test regions. The model was set to compare the tubes ET 10001 (L=15.7 lpmm, T_r=0.6) and R2148MODAX0568 (L=78.7 lpmm, T_r=0.35) as examples of a relatively coarse mesh versus a fine one.

8.1 Gain

Figure 9a shows the resulting gain curves for the two tubes up to B=4.0T. Figure 9b shows the gain vs B curves for all three R2148 experimental variants (0568: L=78.7, T_r=0.35; 0553: L=59.1, T_r=0.46; 0566: L=98.4, T_r=0.32)

8.2 Excess Noise Factor

Figure 10 compares the model predictions for F in the case of the ET 10001 and the Hamamatsu 0568 up to B=4.0T. The Brunel experimental data for the ET device is also plotted.

The corresponding SERFs for the two VPTs at B=4.0T are plotted in figures 11a and 11b for comparison with the B=0 cases in figure 8. The degradation responsible for the increase in F is clearly visible.

9. DISCUSSION

9.1 Gain at B=0

The gain at B=0 is determined to first order by the secondary emission coefficient of the dynode and the transparency of the anode mesh. The beta backscattering on the anode has a second order effect (more backscattering means less gain). With the backscattering fractions for both the dynode and anode set to 0.2, the match to the experimental gain curve of the ET 10001 observed in figure 2 is obtained with a secondary emission coefficient of 35.9 and a scale energy of 304eV. With the same parameters the gains of the other VPT configurations all match reasonably well to quoted values (≈10%). This is quite encouraging in view of the large range of anode transparencies involved (0.3 - 0.7).

9.2 Gain at B<0.5T

In the region of B=0.1T the cyclotron radius of the SEs is of the order of the mesh "holes" and the model predicts strong effects due to the focussing which occurs when the electron flight time is an integer multiple of the cyclotron period τ. The two main independent focussing conditions apply in region 2 (the anode dynode gap) (i) when the flight time of the PEs from the anode to dynode is $n\tau$ and (ii) when the returning SEs fulfill the same condition. Since the two flight times differ by approximately a factor of two (the PEs are on average much faster) this leads to a beat of two frequencies with an extra deep dip when the two conditions coincide. The model results in figure 4a show this effect very clearly.

The dip in the gain is caused by the fact that, in this region of B the focus condition ensures that a photo-electron passing through a mesh hole at position y,z produces the SEs on the dynode at the same y,z position and they are in turn refocussed back onto the same y,z position in the anode plane, thus guaranteeing that they miss the anode mesh. A further resonance condition in the reflection motion in region 1 can ensure that these electrons pass back through the mesh and bury themselves in the dynode.

Clearly this focussing depends on the precision of the structure and the uniformity of the magnetic field. Figure 4b shows the model results when an RMS error of 0.05mm is included in the anode position and a 5% (RMS) non-uniformity is applied to the B-field (in amplitude only, not in direction). The resonant behaviour is damped out somewhat but is still stronger than that observed in the experimental measurements. The possibility that the anode mesh could be fabricated from Ni opens up the potential for the mesh to move in the magnetic field and so wash out the resonant structure.

The longitudinal velocity component of the SE velocity acts to disrupt the focussing effect by varying the flight time of the electrons. As B increases so τ decreases and the focussing is less pronounced. Also the cyclotron radius (ρ) is decreasing to values less than the mesh hole width and so, for both these reasons one expects the resonant effects to die away with increasing B. The experimental data (figure 4a,b) show that this is the case although the resonances in the model seem to die away more slowly.

9.3 Gain at B>1T

By B=1.0T, ρ(SE) has decreased to a value smaller than the mesh hole width (in most cases) and the electrons move spirally "along the rails" of the B-field. The consequence of this is that only PEs which cross the anode plane within approximately ρ(SE) of the edge of a mesh wire have any chance of being intercepted by the mesh. This constriction of the motion to within a few microns of the wire edges tends to invalidate the assumptions about the E-field made initially in order to calculate the motion.

Two asymmetries affect the electron motion near the surface of a wire: (i) the E-field is generally about twice as strong in region 1 as in region 2 which leads to a focussing effect of the field lines from the dynode onto the anode wires, and (ii) the SEs possess only about 200eV on arrival at the anode compared with the 900eV of the PEs making them less stiff and more able to feel the attractive force deflecting them towards the wires. In order to take this effect into account the mesh was assigned a lower transparency for SEs approaching from region 2 than the geometric value. Experimentation showed that using $0.7T_r$ (T_r = geometric transparency) for the reverse transparency reproduced the behaviour of the gain at higher B-fields rather well.

This modification makes very little difference to the gain at B=0 but does reduce the model's sensitivity to B-field. Within the limited data available this parameterisation seems to work for all the VPT designs for which data is available. Thus in spite of the rather *ad hoc* nature of this parameter it does seem to work satisfactorily.

Figure 5 shows the model data for the relative gain of one of the RIE tubes plotted against the experimental measurements out to B=1.4T. The model seems to fit reasonably well with the presence of the resonances below B=1T as the dominant discrepancy. The model data is continued out to B=4.0T and predicts a magnetic hardness of the gain of 0.52 at this field.

Using the parameters measured at Brunel for the standard Hamamatsu R2148 the model gives the relative gain curve shown in Figure 6a. Allowing a 5% non-uniformity in the magnetic field washes out the resonances with the finer mesh, but the shape of the curve does not agree with Hamamatsu's published data. The much poorer performance for whole-cathode illumination tends to make one suspect that structural ferro-magnetic effects are at work.

As with the standard R2148, so with the development model (figure 6b) we get a poor match between the exact shape of the relative gain curve and the model, though the magnitude of the excursions is similar ($\approx\pm1\%$) and also the long-term decline.

Using the model to explore the gains of the different VPT designs out to B=4.0T we find that (figure 9a) the fine mesh R2148MODXA0568 ($L=78.7mm^{-1}$,$T_r=0.35$) shows a much better magnetic hardness of 0.63 at B=0.4 compared with the E/T 10001 ($L=15.7mm^{-1}$, $T_r=0.6$) at 0.43. However the gains at B=4.0T are almost identical (6.7, 6.2 respectively) due to the much lower initial gain of the fine mesh tube.

Similarly figure 9b shows that the model predicts that there is little to be gained from decreasing the mesh pitch much further since the gain ends up at 6.7 for all the R2148 protoypes (L=59.1, 78.7 and 98.4 mm^{-1}). It is interesting to note that the cyclotron resonances are universally preserved at a low level right out to 4T in the case of the fine meshes. This is almost certainly because the secondary electrons are almost all collected in the first pass of the anode and the very small mesh holes (5.8 microns for the smallest) are small enough to be comparable with ρ(SE).

9.4 Excess noise factor

In figures 7a and 7b are seen the comparison between the model predictions and the Brunel experimental measurements on E/T 10001 of the behaviour of the excess noise factor as a function of B-field in two different bias conditions. While there is a small but systematic discrepancy in the 800V/700V results the 600V/500V agree quite well. The reason for the discrepancy will require further study but, as a first result the level of agreement seems to indicate that the model cannot be far wrong.

The model single electron reponse function (SERF) of E/T 10001 at B=0 (800V/700V) is shown in figure 8a. There is a satisfactory gaussian peak for the PEs that make it to the dynode and it is clear that a large contribution to the standard deviation of the distribution (and hence F) is made by the 713 samples (36%) of one-electron events. These are attributable to PEs impacting the anode on the way to the dynode. The fraction (36%) is slightly less than 1-T (40%) because of backscattering off the anode giving a few electrons a second chance.

The Brunel measurements on the Hamamatsu XA0568 tube showed F values in the region of 2.5 at B=0. The model SERF for this tube (figure 8b) shows why this is so. In this case we have 1226 samples of single electron events (61%) which is (as above) just slightly less than 1-T (65%).

In figure 10 the model is used to extrapolate the excess noise calculations for E/T 10001 and Hamamatsu XA0568 up to B=4T. The available experimental data are shown for comparison. While figure 9a shows that there is little to choose between the gains of the two tubes at 4T the model indicates that F is 50% worse for the E/T device at 4T compared to the Hamamatsu tube. The gain change of the latter over the range of B field is also smaller. The fine mesh VPT thus shows superior magnetic hardness of both the gain and the excess noise factor although the gains of both tubes are comparable at B=4T.

Figures 11a and 11b show the SERFs for the two tubes corresponding to the 4T cases in figure 10. In both cases the nice gaussian has been destroyed by the poor collection. It was noted in the B=0 case that F is strongly affected by the number of single

electron events. In figure 11b it is seen that this number has not changed (within statistics) and the number of zeros is also similar to B=0. However, by contrast the E/T tube has acquired a very large number of zeros in addition to an increased number of singles (figure 11a). This accounts for the larger F value. The null events are caused by the increased probability of SEs spending the whole of their existence in the tube shuttling up and down through the large mesh holes until all their energy is dissipated in the dynode.

10 CONCLUSIONS

In general it appears that the monte-carlo model is capable of modelling the essential behaviour of VPTs in axial magnetic fields. While agreement is not perfect in all the cases considered, the basic trends of the gain and excess noise factor with B-field seem to be well represented. The model predicts that a tube with a fine anode mesh will be superior to one with a coarser mesh in respect of performance at high B field. The low transparency which (for practical reasons) accompanies a low mesh pitch value leads to the fine mesh tube having a lower gain (G) and a higher excess noise factor (F) at B=0 compared to the coarser (more open) mesh tube (figure 9a). However, as the B field climbs above 1T the fine mesh version shows less relative gain change and the excess noise factor (figure 10) rises much less than in the coarse mesh version. Thus, as a practical device, the fine mesh tube is to be preferred in spite of the fact that the gains are comparable at B=4T.

The question of how fine to make the anode mesh is answered by figure 9b which shows the gain curves of three Hamamatsu prototypes with L=59.1, 78.7 and 98.4 lines/mm. While the final gain at B=4T is essentially invariant, the average dG/dB improves significantly between L=59.1 and L=78.7. The gain from the final step to L=98.4 would seem to be marginal. Thus the Hamamatsu R2148MODXA0568 (L=78.7, T_r=0.35) and R2148MODXA0566 (L=98.4, T_r=0.32) are both probably acceptable.

While it is obvious that the precise modelling of the interactions of the electrons in a VPT is a very complex business, experience with the montecarlo model has shown that a crude geometric model of the response of the device to increasing axial B field can be visualised. At high fields (B>1T) the cyclotron radius of the photoelectrons is in the range of 1μm, and so one can envisage their trajectories as straight lines from cathode to dynode, i.e. a contact print of the anode mesh is made on the dynode. The cyclotron radius ρ of a typical SE moving back towards the anode mesh is a few microns. Thus any SE originating further from the edge of a mesh wire than ρ will generally miss the anode mesh and oscillate in the mesh gap until its energy is spent in the dynode.

One can interpret the effect of this as restricting the effective area of the photocathode to a window frame of width ρ just inside a mesh hole (figure 12), instead of (at low B) the whole open area of the mesh hole and can quantify the relative gain R(B) = G(B=B)/G(B=0) as the ratio of the area of the window frame to the area of the mesh

hole. Evaluating this (assuming a rectangular hole) in terms of the usual mesh parameters gives:

$$R(B) = 1 - (1 - 2L\rho/\sqrt{T_r})^2$$

where: $\rho = mv_T/Be$

Decreasing the second term in the brackets causes R(B) to decrease. Thus increasing B decreases the gain while increasing L and decreasing T_r reduces the sensitivity of the expression to changes in B. Clearly these trends reproduce the general behaviour noted in the montecarlo calculations. Due to the fact that ρ is a function of the transverse velocity component (v_T) and hence of the wide spectrum of SE energies (figure 3) and emission angles, one cannot derive exact numbers from the "window fame" model; however, the general trends inherent in the physical situation are well represented as illustrated in figure 13. Averaging R(B) over the secondary emission energy spectrum and including a $\cos\theta$ polar angular distribution for the emitted electrons at B fields high enough for ρ to be smaller than the mesh hole diameter gives the relative gain curves shown in figure 13. The considerable underestimate in the case of the coarse mesh tube (E/T 10,001) shows the importance of multiple transits of the SEs in the case of a high transparency giving repeated chances of generating a detectable electron.

While a number of parameters require to be inserted semi-empirically into the montecarlo calculations, the fact that the same parameter set works to first order with all tube designs gives one considerable confidence in the calculations. Clearly the processing of the dynode will yield variations in ε_{max} which will reflect directly in the gain of the tubes. This parameter, however, does not affect the magnetic hardness of the tubes.

It is thus hoped that while improvements to the model will be implemented as experience with it increases, it can form a viable basis for the analysis of the experimental data now being generated and contribute to the optimisation of VPT design for the ECAL application.

The next development step for the model is to permit angled B-fields. This is more complex but still a reasonable calculation. The problem of accounting for any magnetic fields caused by the polarisation of structural materials is on an altogether different scale and is likely to be too complex for easy calculation.

REFERENCES

[1] F.Sauli; Principles of operation of multiwire proportional and drift chambers, CERN 77-09, p 52 and G. A Erskine Nuclear Instrs. and Methods **105**, 565 (1972)

[2] R. W. Dressler; Retrofugal electron flux from massive targets irradiated with a monoenergetic primary beam. Phys. Rev., **144**, 332.

[3] R. Kollath; On the energy distribution of secondary electrons. Ann. Phys. Lpz., **39**, 59.

[4] H Bruining, Physics and Applications of Secondary Emission, Pergamon Press, London, 1954.

FIGURE CAPTIONS

1. A sketch of the structure of a VPT. The biassing convention used in the model is that V_c and V_d are negative with the anode at earth.

2. A comparison of the gain versus dynode potential as measured on the E/T 10001 tube at Brunel with the monte-carlo model with the parameters specified. The anode-dynode potential difference is >200V for all points to assure complete collection of the secondaries.

3. A typical secondary electron spectrum generated by the model for the case of a CsSb dynode. A logarithmic scale is used vertically to show the large dynamic range.

4. (a) This figure compares the measured and modelled gain versus B-field curves for E/T 10001 at two different bias conditions. (b) The same data modelled with experimental “imperfections” i.e. a 50μm RMS error in the anode position and a 5%RMS non-uniformity in the magnetic field.

5. The relative gain of the RIE tube FEU-189-N37 modelled for comparison with the experimental data as a function of B-field.

6. (a) The relative gain of a standard Hamamatsu R2148 as predicted by the model and compared with the data sheet curve. (b) The relative gain as modelled for the Hamamatsu R2148MODAX0568 and compared with the Brunel measurements up to B =0.4T.

7. The excess noise factor modelled for the E/T 10001 tube compared with the Brunel measurements at (a) 800V/700V and (b) 600V/500V.

8. The single electron respose functions (SERF) modelled at B=0 for (a) E/T 10001 and (b) Hamamatsu XA0568.

9. (a) The gain as modelled out to B=4T for E/T 10001 and Hamamatsu XA0568. (b) The gains of the three Hamamatsu development tubes modelled out to B=4T.

10. The excess noise factor modelled out to B=4T for the E/T 10001 and Hamamatsu XA0568. The available experimental points are plotted for comparison.

11. The single electron response functions modelled at B=4T for (a) the E/T 10001 and (b) the Hamamatsu XA0568.

12. A schematic model of the window frame model for the gain of a VPT.

13. A comparison of the relative gain at high B fields as calculated from the full montecarlo model and the window frame model.

FIGURE 1

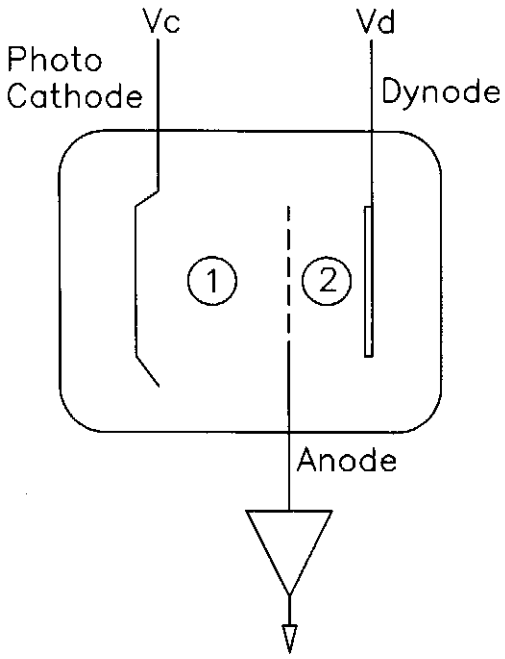

Typical Bias Conditions:

Model	-800V	0V	-100V
	-600V	0V	-100V
E/T Data	0V	+600V	+500V
	0V	+800V	+700V

FIGURE 2

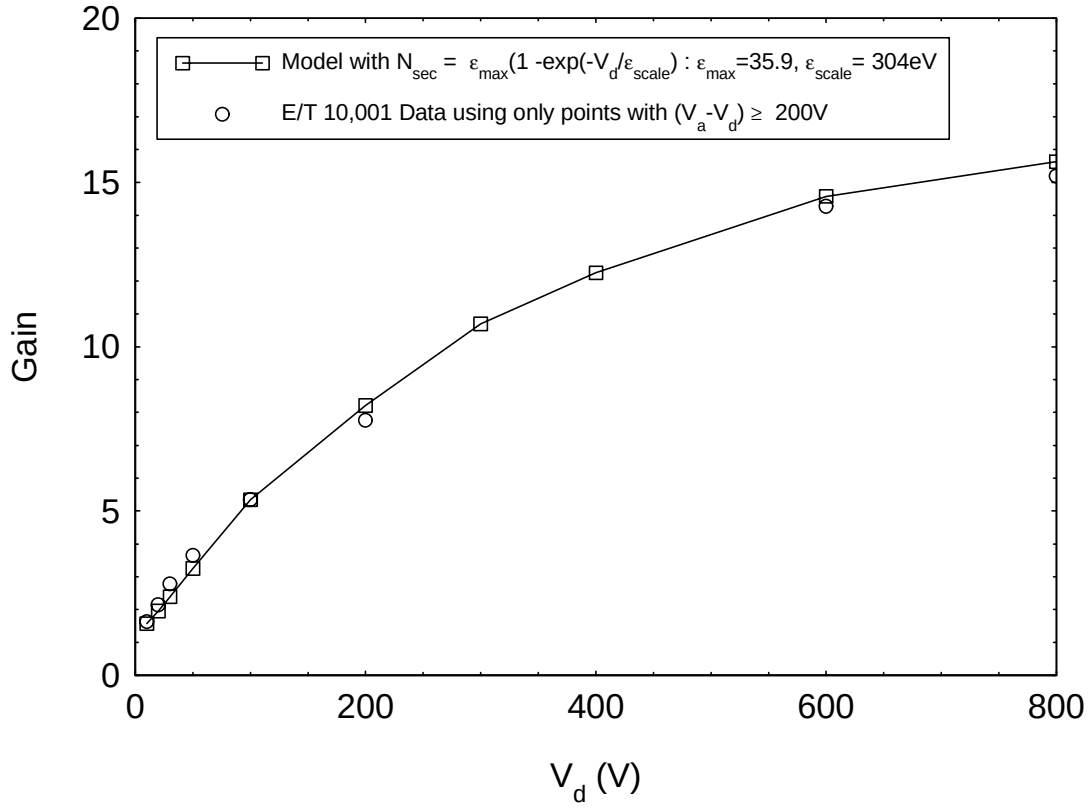

FIGURE 3

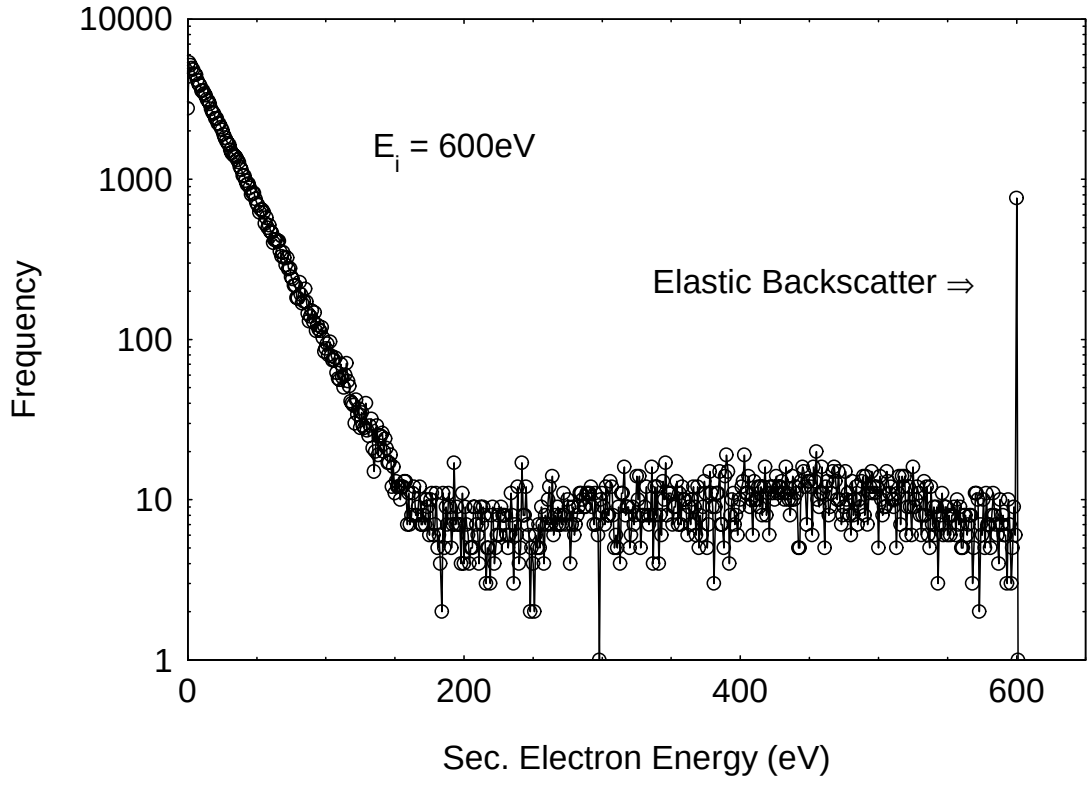

FIGURE 4a

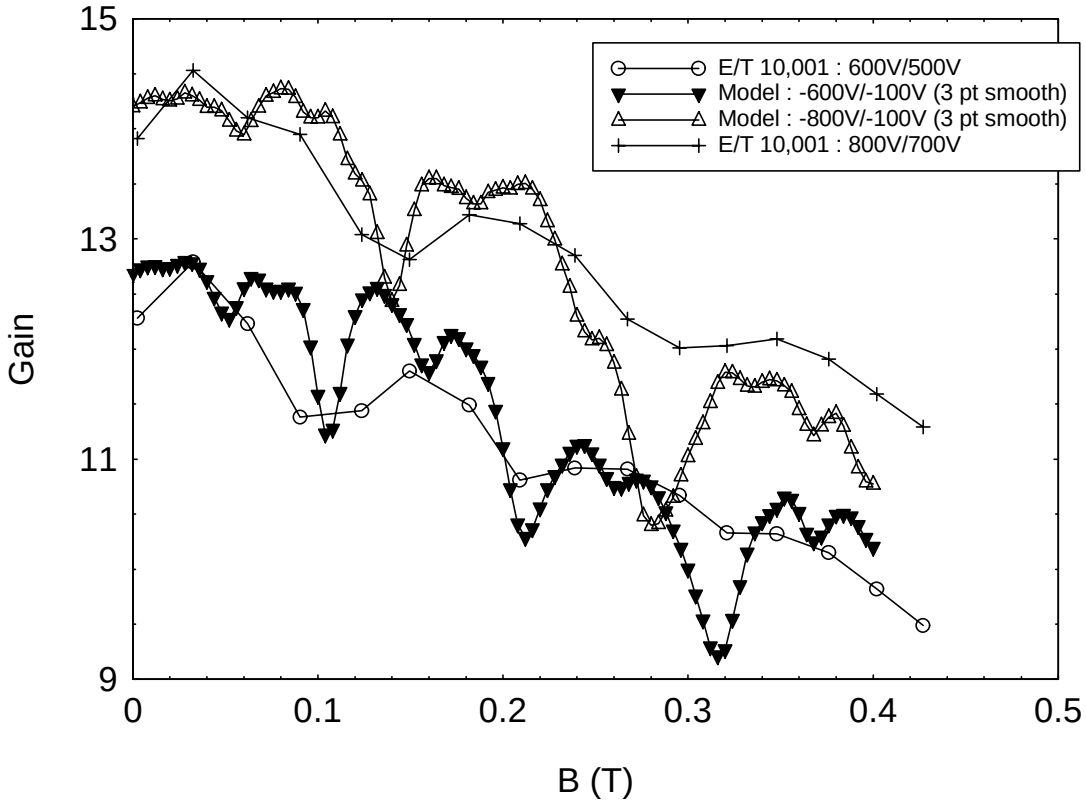

FIGURE 4b

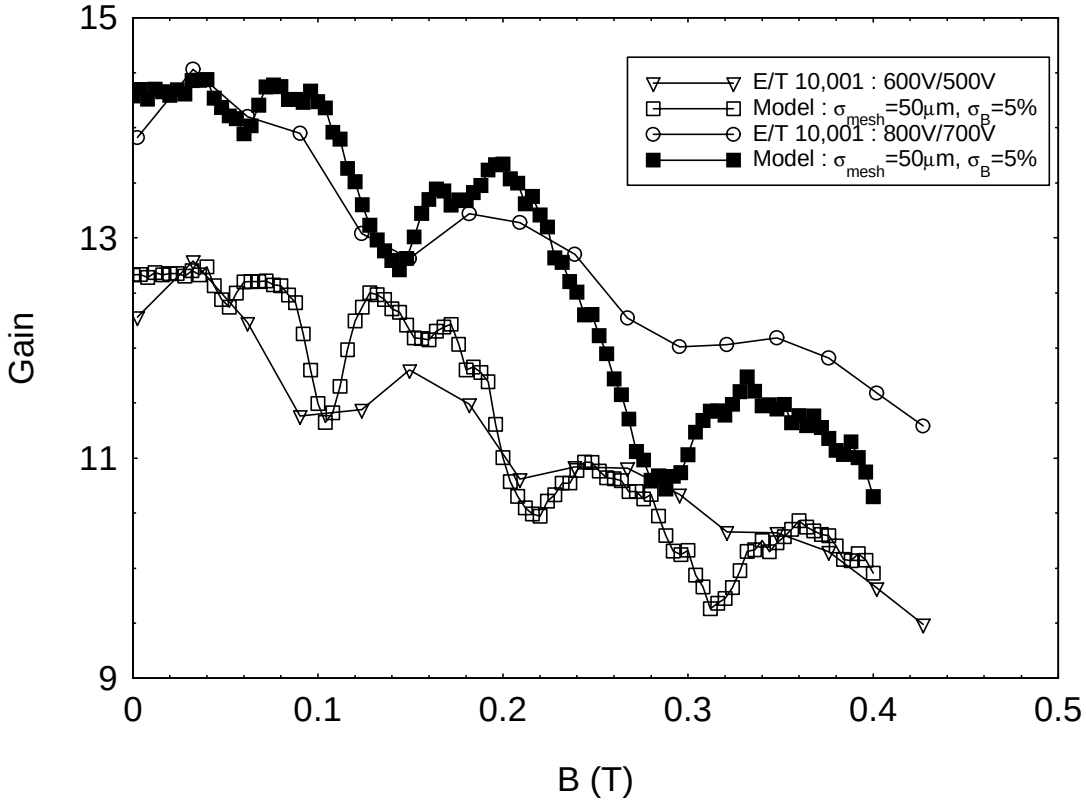

FIGURE 5

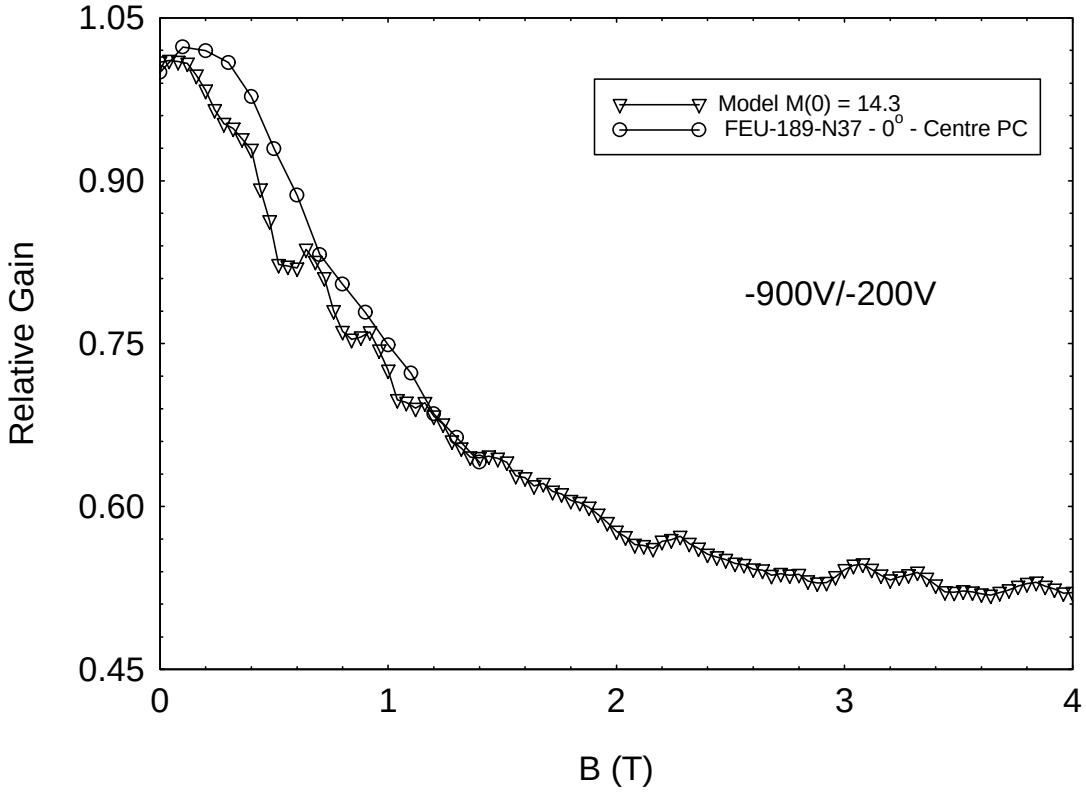
1.05
0.90
0.75
0.60
0.45
Relative Gain
0
1
2
3
4
B (T)
Model M(0) = 14.3
FEU-189-N37 - 0° - Centre PC
-900V/-200V

FIGURE 6a

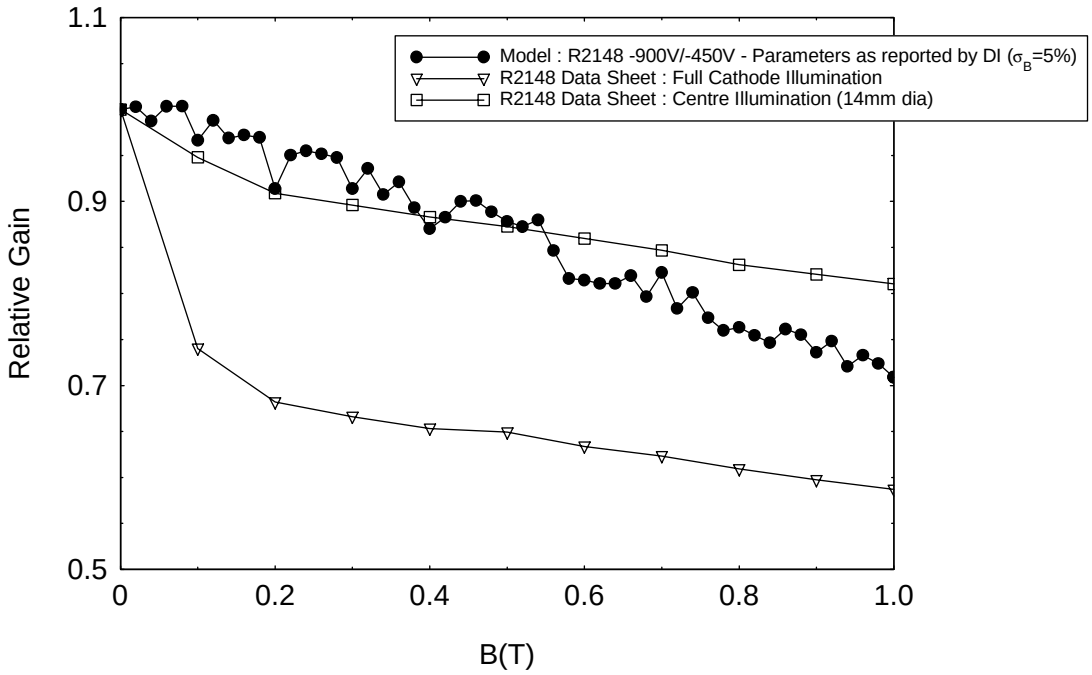

FIGURE 6b

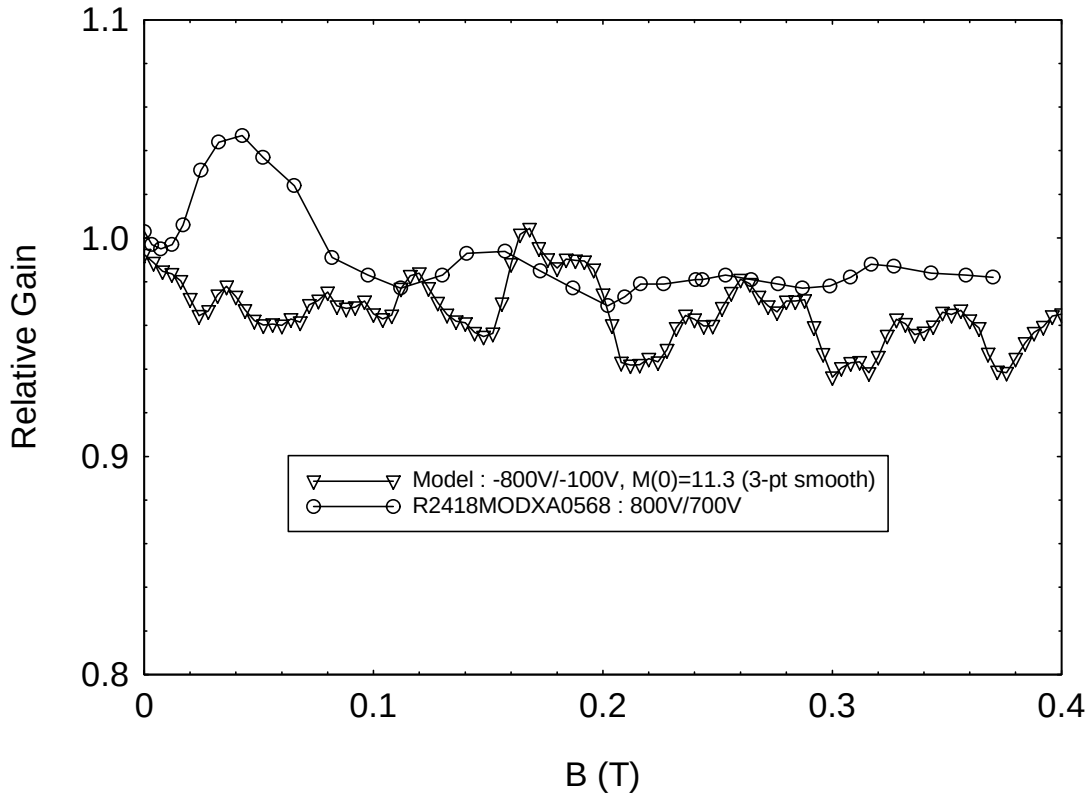

FIGURE 7a

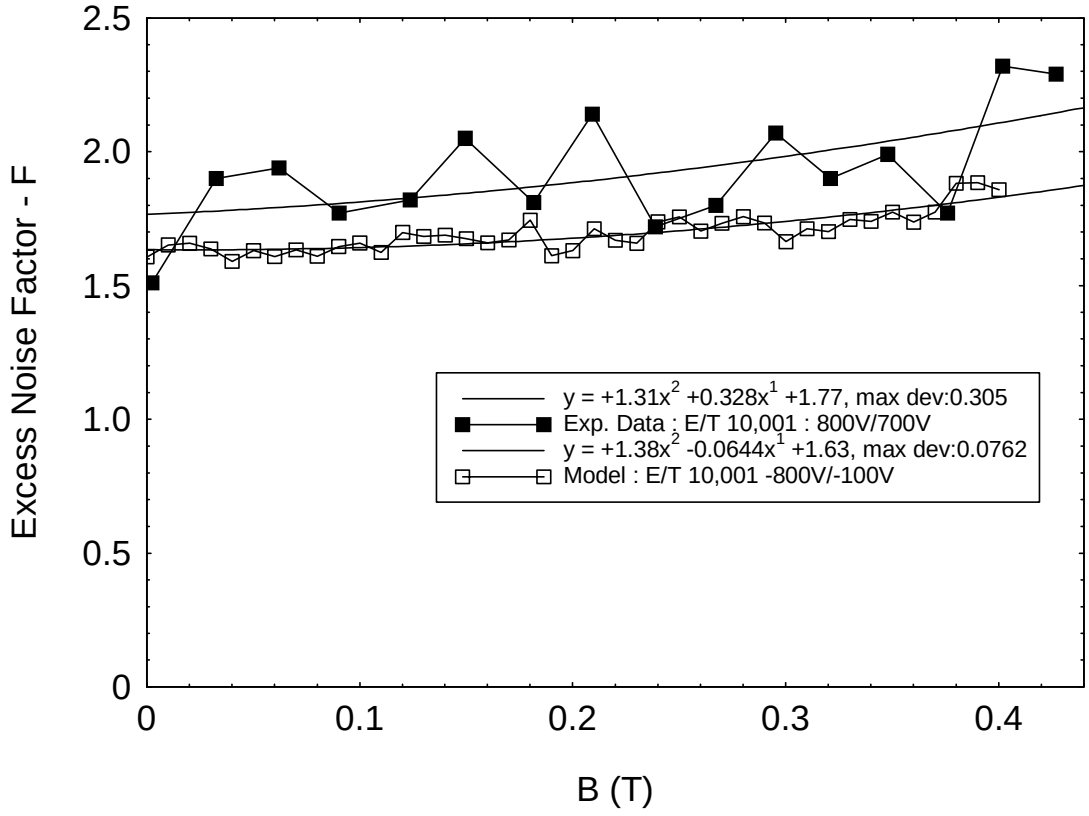

FIGURE 7b

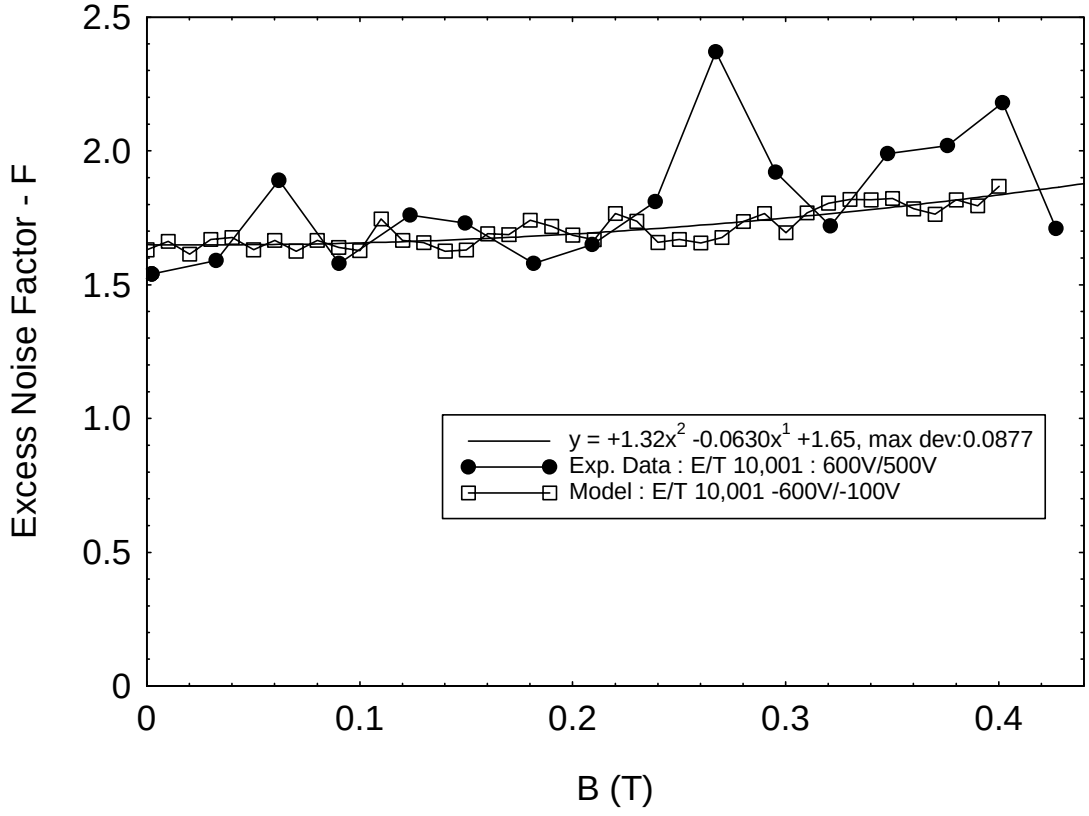

FIGURE 8a

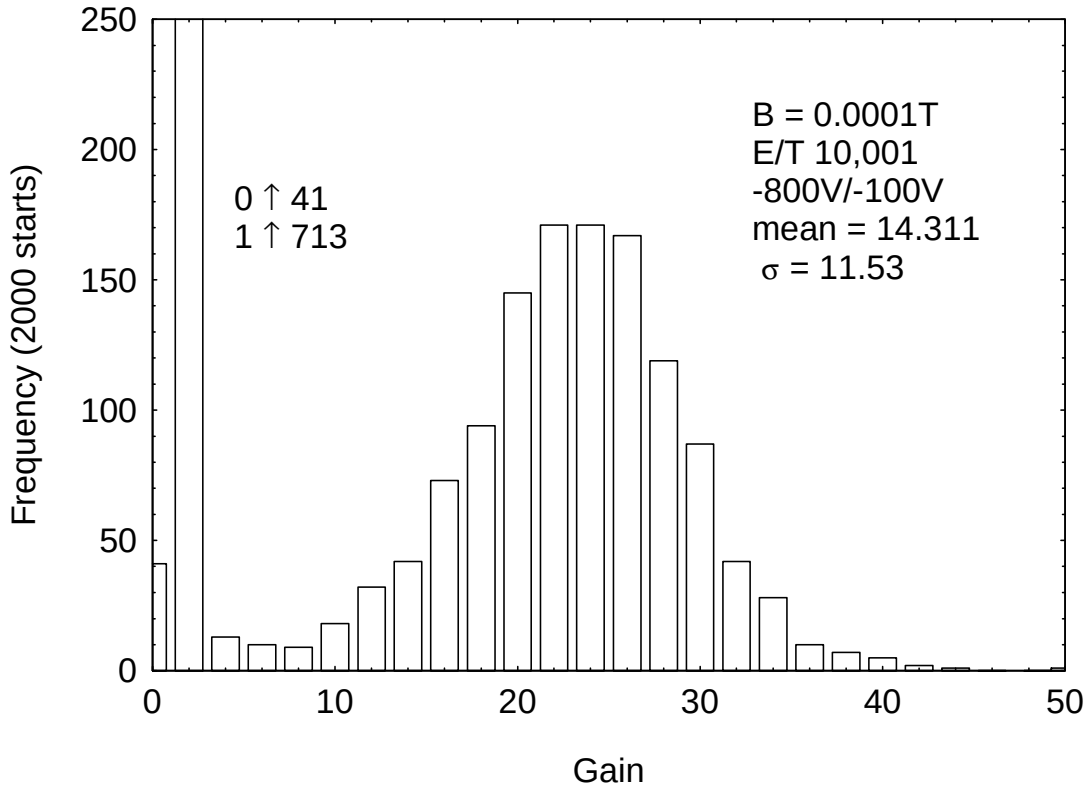

FIGURE 8b

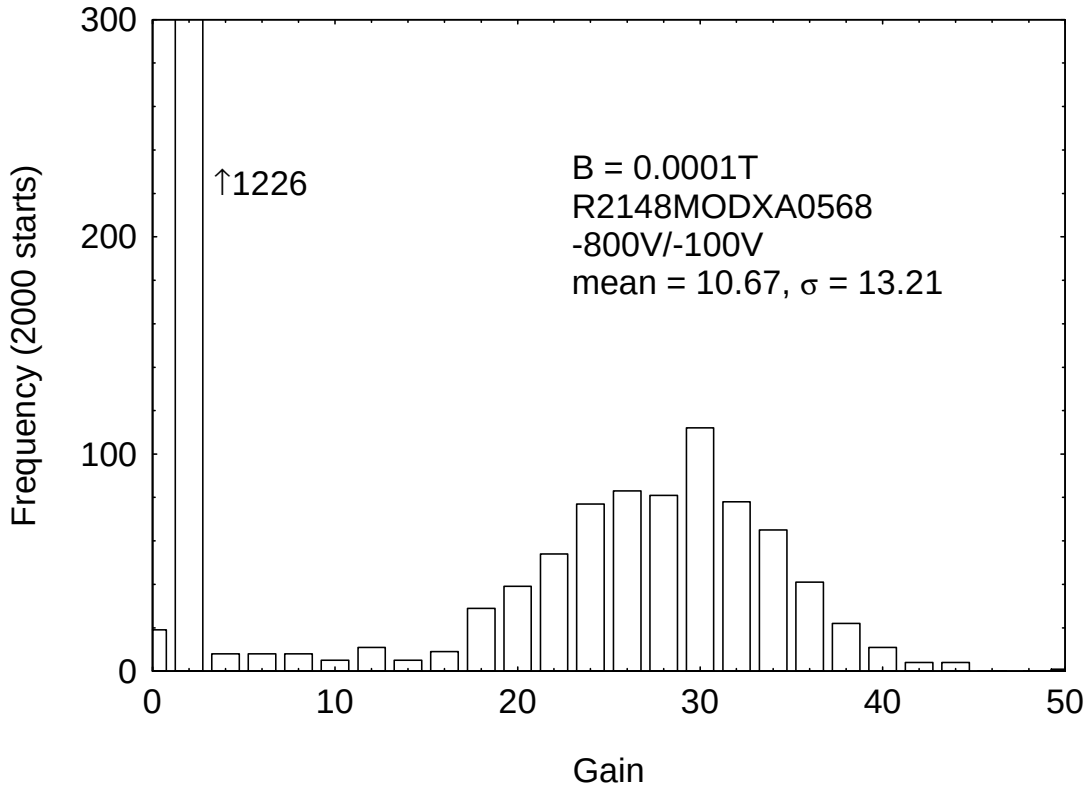

FIGURE 9a

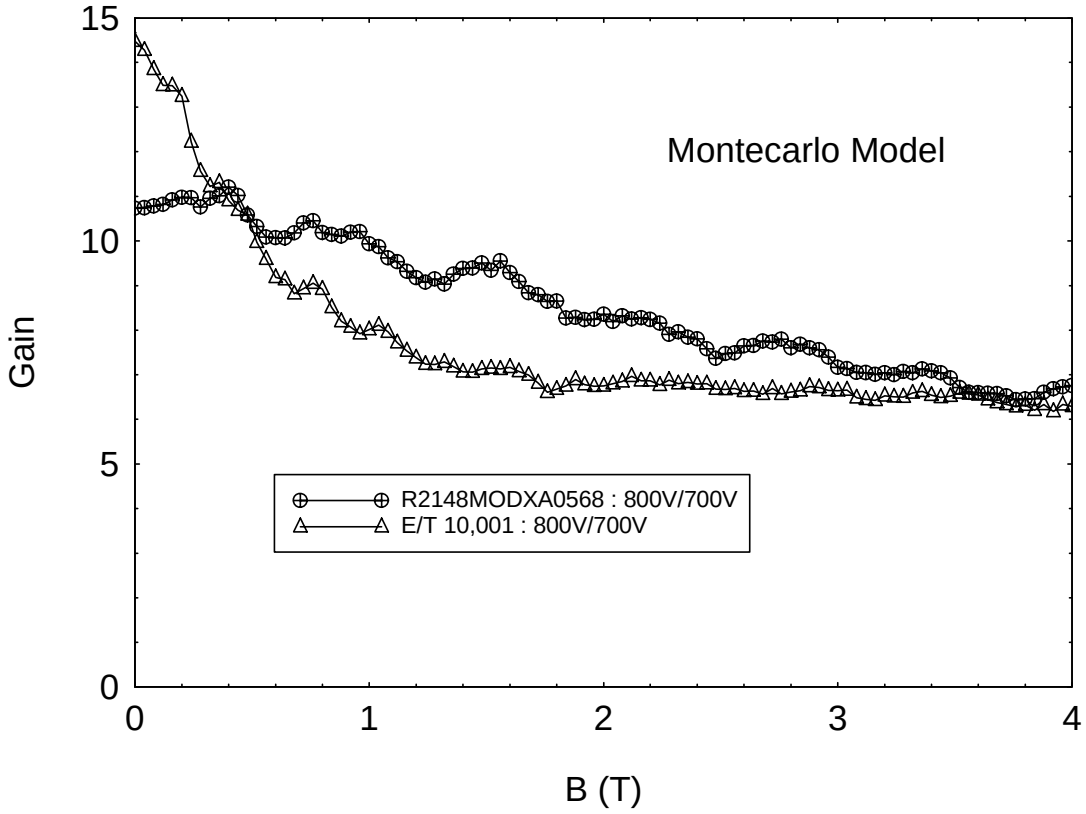

FIGURE 9b

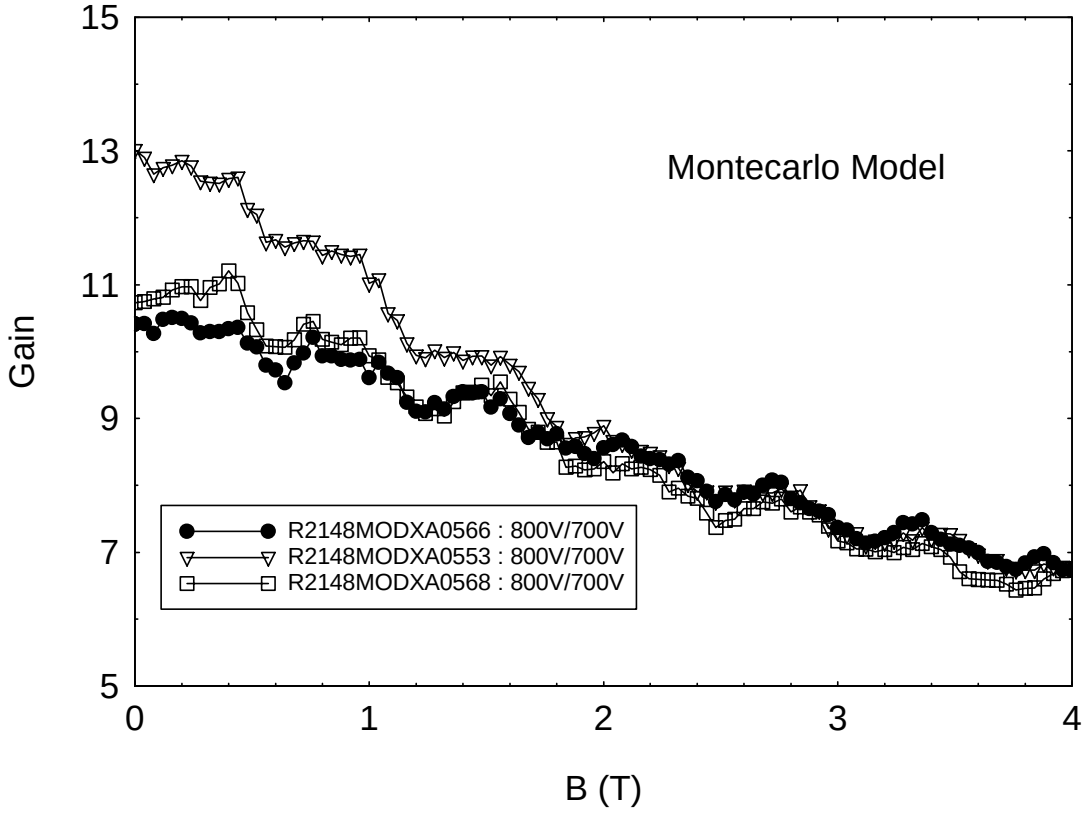

FIGURE 10

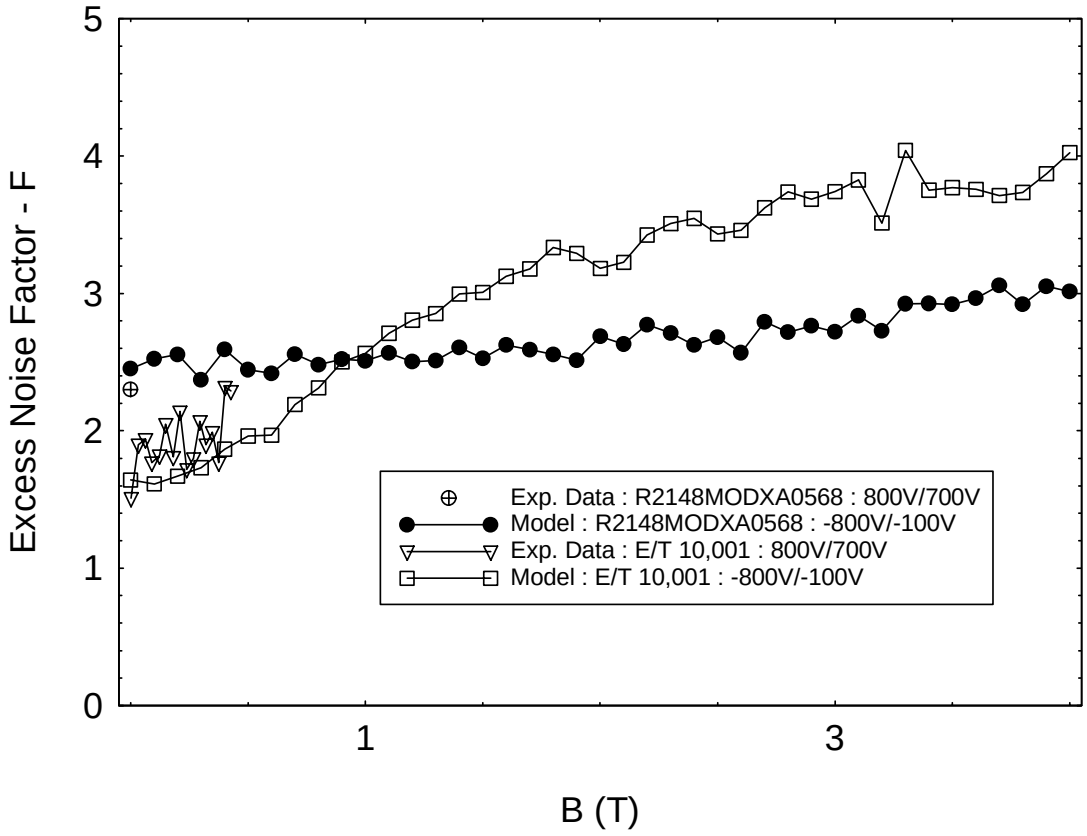
Excess Noise Factor - F
5
4
3
2
1
0
1
3
B (T)
Exp. Data : R2148MODXA0568 : 800V/700V
Model : R2148MODXA0568 : -800V/-100V
Exp. Data : E/T 10,001 : 800V/700V
Model : E/T 10,001 : -800V/-100V

FIGURE 11a

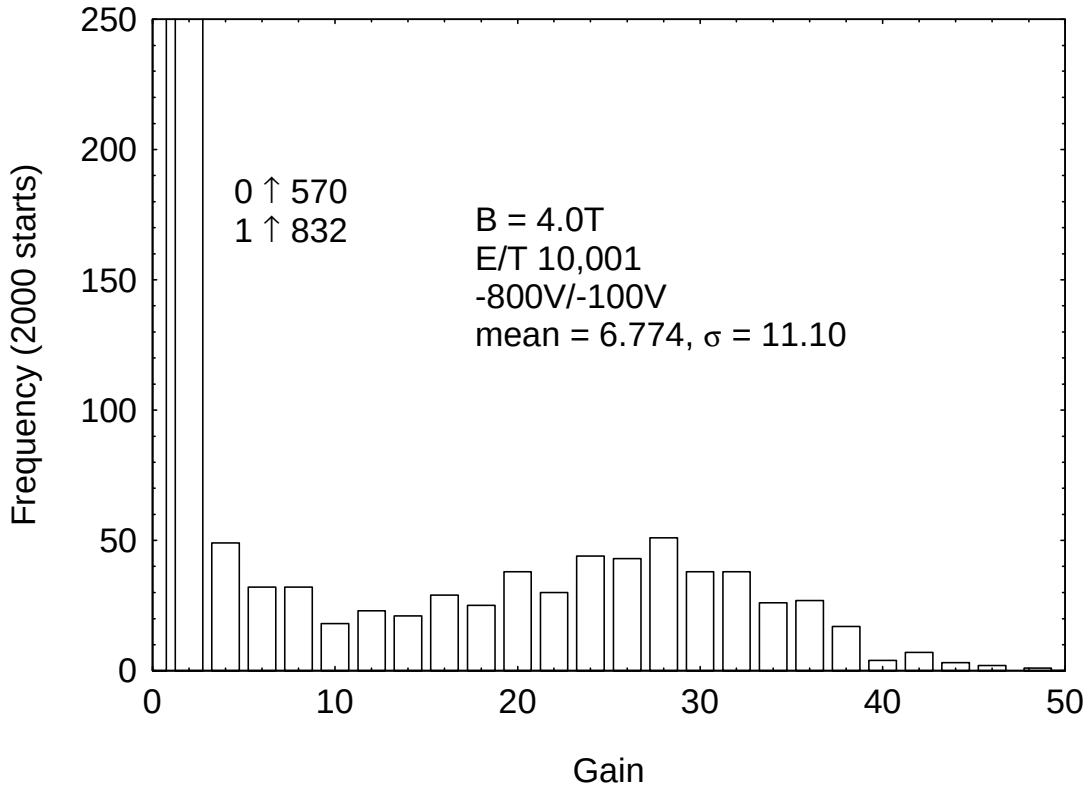

FIGURE 11b

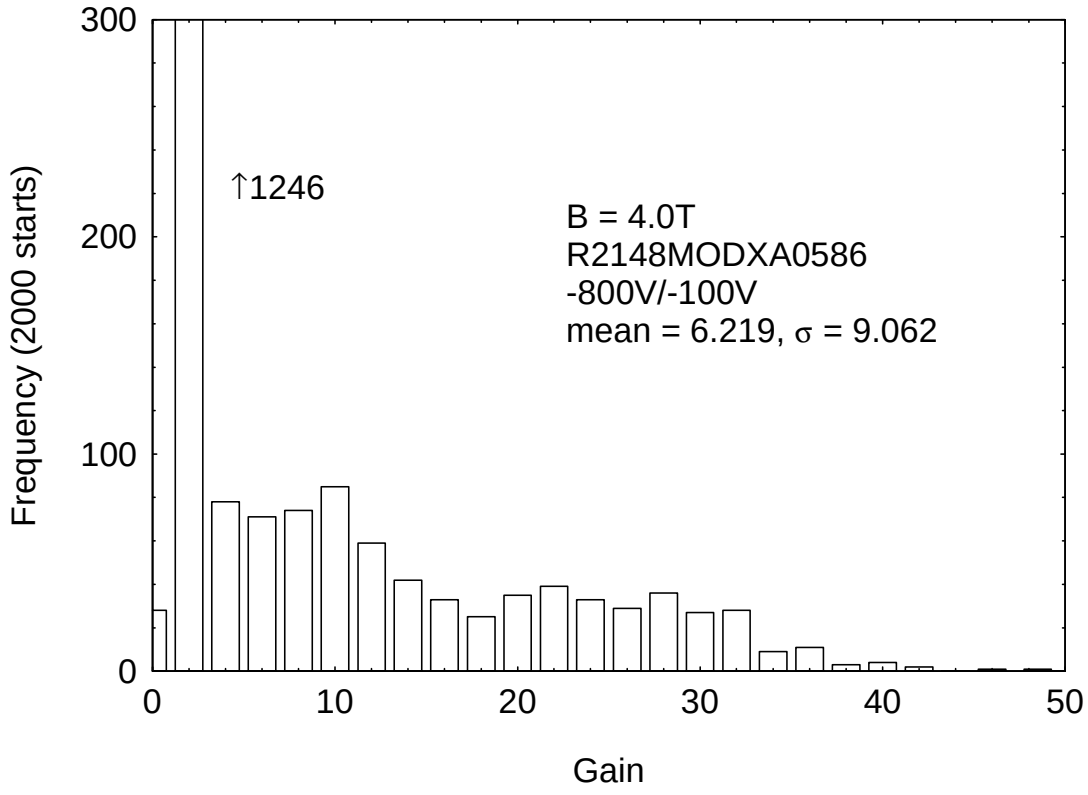

FIGURE 12

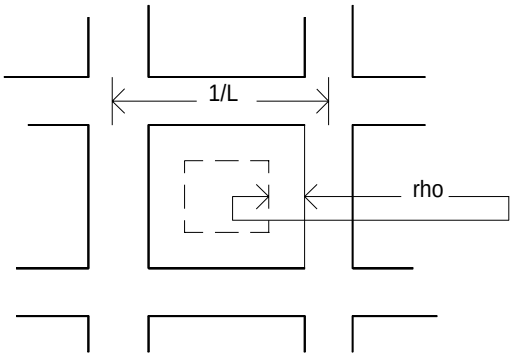

FIGURE 13